

CARRIER DRIFT AND DIFFUSION CHARACTERISTICS OF Si PARTICLE DETECTORS MEASURED *IN SITU* DURING 8 MeV PROTON IRRADIATION

E. Gaubas^a, T. Čeponis^a, J. Vaitkus^a, and J. Raisanen^b

^a Vilnius University, Institute of Applied Research, Saulėtekio 9-III, LT-10222 Vilnius, Lithuania

E-mail: eugenijus.gaubas@ff.vu.lt

^b Division of Materials Physics, Department of Physics, University of Helsinki, Finland

Received 13 June 2011; revised 18 November 2011; accepted 1 December 2011

The carrier drift and recombination parameters determine the functional characteristics of Si high energy particle detectors. In this work, techniques for the *in situ* control of drift–diffusion current transients during 8 MeV proton irradiation are discussed. The characteristics obtained in silicon particle detectors and carrier drift–diffusion and generation parameters variations during proton exposure are analysed. The models of current transients within a depleted diode with the drifting-induced charge domain at low and high densities of light excited excess carriers within the diode base region have been proposed. A small impact of radiation defects on carrier drift/diffusion parameters and more complex variations of excess carrier recombination / trapping lifetimes during irradiation have been revealed.

Keywords: carrier drift, diffusion and recombination, current transients, particle detectors, radiation defects

PACS: 72.20.Jv, 71.55.Eq

1. Introduction

The evaluation of the mechanisms of radiation damage of particle detectors in the range of low and moderate (10^{12} – 10^{14} cm⁻²) fluences is commonly implemented by combining several techniques. Examination of leakage current, of carrier generation lifetime by thermally stimulated current (TSC) [1], by deep level transient spectroscopy (DLTS) [2, 3] and by exploiting measurements of current transients (TCT) [4–8] is employed in the analysis of the post-irradiation state of devices. The evolution of radiation defects and their manifestation in operational parameters of particle detectors is important. Therefore, simultaneous control of the changes of carrier drift and recombination/generation parameters during irradiation is desirable. This allows evaluating the operational frequency/dielectric relaxation rate, the impact of bulk serial resistivity and other parameters of particle detectors within operational conditions when irradiation fluence increases.

In this work, techniques are presented for *in situ* monitoring of the carrier recombination and drift parameters during irradiation by 8 MeV protons. The results of simultaneous measurements of microwave probed photoconductivity transients [9] combined with injected charge induced current transients and of steady-state generation current are briefly reported.

2. Instrumentation for measurements and samples

The experimental arrangement for the remote measurements of the microwave-probed photoconductivity transients (MW-PCT) and induced charge diode current (ICDC) signals is designed on the basis of the instrument for MW-PCT implementation described in [9]. The additional components and biasing circuitry installed within this MW-PCT-E instrument are sketched in Fig. 1. The transient MW-PC and ICDC signals are synchronously

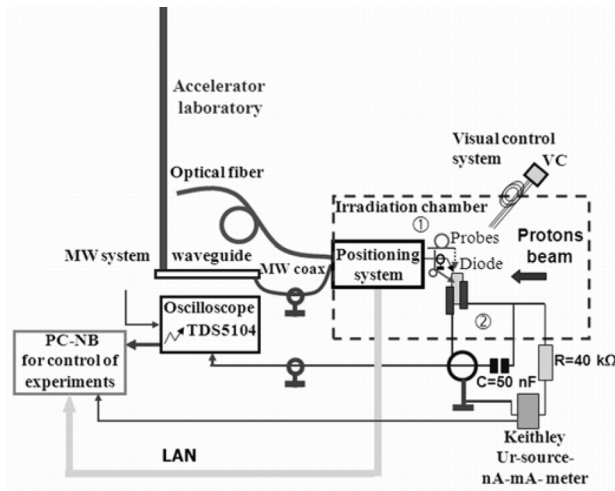


Fig. 1. Sketch of a set-up for the simultaneous measurements of carrier drift and recombination characteristics under applied bias during irradiation by a proton beam: 1 excitation fiber-tip and microwave (MW) needle-tip probes for contact-less measurements of the microwave-probed photoconductivity (MW-PC) transients, 2 circuitry for electrical biasing and injected charge drift (ICDC)/injected charge collection (IChCC) currents registration inside vacuumed irradiation chamber.

registered outside the accelerator control area on different channels of the 1 GHz Tektronix TDS-5104 oscilloscope, using 50Ω load resistors. The proton beam current was kept rather small (about 0.5 nA) to minimise noise within the ICDC signals and to avoid the excess carrier induced impact ionization avalanche breakdown effect inherent for elevated proton fluxes [10]. The diode leakage current (dc) was synchronously measured using Keithley voltage source/electrometers. Various regimes of simultaneous measurements of the injected charge induced diode current (ICDC) and injected charge collection (IChCC) transients have been employed. Measurements were carried out at $T = 300$ K.

The detectors fabricated from Czochralski (Cz) Si with (p^+n-n^+ and n^+p-p^+) diode structure had an active area of $5 \times 5 \text{ mm}^2$ and thickness of $300 \mu\text{m}$ [10]. A special sample holder was designed to enable proper electrodes for the electrical circuitry, containing windows for the proton beam and optical excitation (Fig. 1). A freshly cleaved cross-sectional boundary of a pad-detector broken into half was used for perpendicular bulk excitation and MW-PCT-E probing by a coaxial needle-tip MW antenna, using a 3D stepper motor driven stage containing a flexible bellow.

3. *In situ* variations of diode currents and microwave-probed photoconductivity

Variations of the injected charge induced diode current (ICDC) transients at excitation intensities necessary to obtain a signal just above the ICDC noise level were measured using 531 nm wavelength surface excitation with 400 ps laser pulses of about 10^{22} fJ , illuminating a non-metallised hole on the diode. In this case, the excitation density is below the threshold for resolving the MW-PC response. The ICDC signals were registered at applied voltages significantly above the full depletion voltage (for which depletion region width is equal to geometrical thickness of a diode base) of non-irradiated diodes ($U > U_{\text{FD}}$). The ICDC transients registered *in situ* at different 8 MeV proton exposure instants are illustrated in Fig. 2(a)

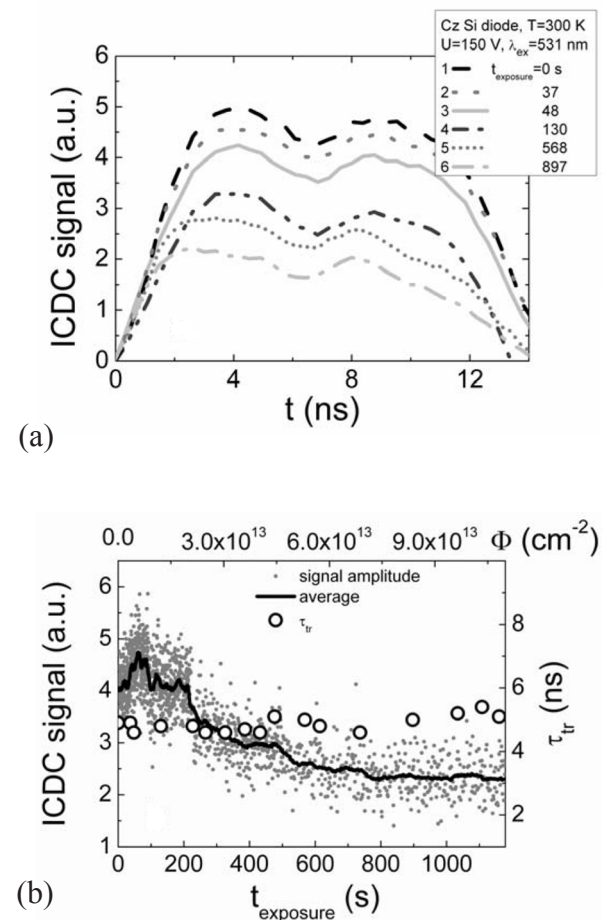


Fig. 2. Variations of (a) induced charge diode current (ICDC) transients and (b) ICDC signal amplitude as well as excess carrier drift time as a function of exposure time measured for 8 MeV protons using the surface excitation regime when carriers are generated in vicinity of the p^+n region of the diode structure (drift of electrons).

for the (531 nm) photo-injected surface charge electrons within the n -base. The shape and duration of the ICDC pulses appear to be approximately invariant with increasing irradiation time.

Elevated surface (531 nm) and bulk (1062 nm) excitation (~ 100 times that of generation of ICDC at the detection threshold) is sufficient in order to register both MW-PC and injected charge collection (IChCC) current signals (on 50Ω load) and to monitor directly the carrier diffusion–recombination parameters. The correlated evolutions of IChCC (a) and MW-PC (b) transients registered simultaneously *in situ* during 8 MeV proton irradiation with a fixed excitation density and applied voltage are illustrated in Fig. 3. A correlated decrease of both IChCC and MW-PC pulse durations as a function of irradiation time is noticed for short exposure times. This implies a rapid reduction of carrier lifetime when its value approaches the carrier transit time across the diode base.

4. Evaluation of carrier drift–diffusion and recombination–trapping parameters

The transient current technique (TCT) [3–6] is widely used in Si detectors characterisation for both under- and over-depletion diode operational regimes. The model of TCT characteristics [3–6] based on the Shockley-Ramo's theorem [11] has

been shown [12–14], however, not to be applicable for under-depleted diodes. In order to understand the nearly independent shape and duration of ICDC transients and to validate the procedures used to extract material parameters, the formation of the injected charge induced diode current (ICDC) transients requires a more detailed discussion. A sketch of the electric field distribution within the n -base of the diode under injected excess carrier pairs ($n_{\text{ex}} = p_{\text{ex}}$) is shown in Fig. 4. For applied voltages $U < U_{\text{FD}}$, current flows in the external circuit due to simultaneous extraction of majority carriers from the electrically neutral n -base and p^+ regions caused by the separation of the injected excess carrier pairs due to the steady-state field and extraction of excess holes from the n -base region into the p^+ region. During this process, the first peak within the ICDC transient appears.

The separation process induces the change of depletion width w_{q^n} (increase relative to its steady-state value w_0) due to the surface field $-q_e/(\epsilon_0\epsilon)$ of excess electrons. The extracted excess holes located at the p^+ -side produce the same value of the surface field. Thus, the overall charge balance ($w_{p^+} N_{A,p^+}^- = w_n N_{D,n}^+$) together with $q_{h,p^+} X_{0,p^+} = q_{e,n} X_{0,n}$ in the diode is maintained. This balance in the n -base is supported by the applied dc voltage (U), together with the surface charge $q_h/\epsilon_0\epsilon$ (in the p^+ layer, $X_{0,p^+} < X_{0,n}$), if the q_e domain is separated by $X_{0,n}$ from the metallurgic

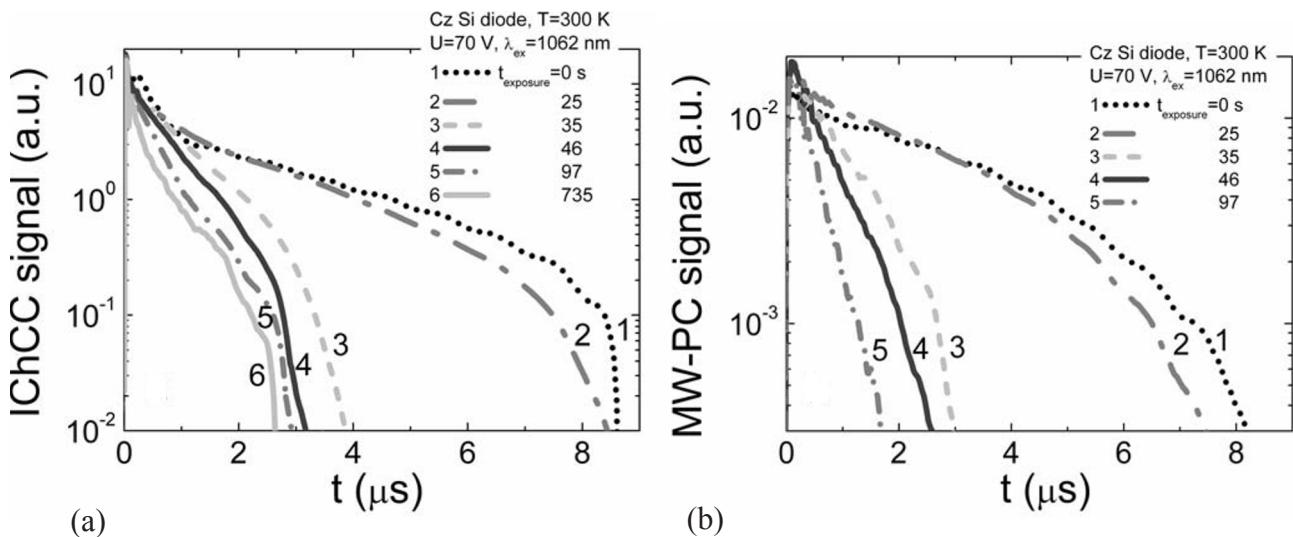


Fig. 3. Variations of (a) injected charge collection current (IChCC) and (b) microwave-probed photoconductivity (MW-PC) transients registered *in situ* during 8 MeV proton irradiation of a Si pad-detector when the bulk excitation density and applied bias voltage $U \geq U_{\text{FD}}$ were fixed.

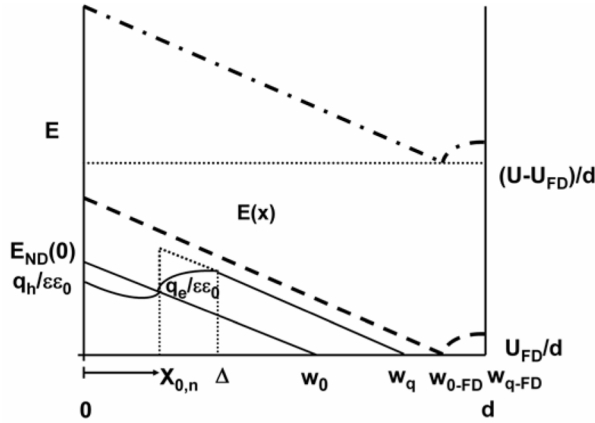


Fig. 4. Sketch of electric field distribution due to induced surface charge for different applied dc voltage values. Dotted and solid lines represent $U < U_{FD}$, dashed line represents $U \equiv U_{FD}$ and $w = d$, dash-dotted line represents $U > U_{FD}$. For $U < U_{FD}$, the enlarged details of field distribution are shown, where dotted line is attributed to an induced surface-charge field $q_e/\epsilon\epsilon_0$, while solid line represents an excess carrier charge domain of width Δ .

boundary within the depleted region w_0 of the n-base. Then for $U < U_{FD}$, using the standard depletion approximation in device physics, e. g. [15, 16], the depletion width is

$$w_q = \sqrt{\frac{2\epsilon\epsilon_0}{eN_{Def}} \left[U + \frac{(\pm)q_e}{\epsilon\epsilon_0} X_0 \right]}. \quad (1)$$

A sketch of the electric field distribution is illustrated in Fig. 4 by a dotted line for a surface charge q_e separated by a length X_0 . Here, a “depletion width” (w_0 , w_q) means trivially that the material is electrically neutral (the potential together with the electric field are zero) at this point, e. g. [15]. The ICDC flows during $q_e(t)$ relaxation (for instance due to capture by deep centres of excess electrons within the depleted n-base region) and changing of the separation length $X_{0,n}(t)$ (e. g. due to the capture of excess holes in the depleted p^+ region and drift) until w_q recovers to w_0 . The latter relaxation process can be found using the condition for a the duration of the domain drift within the space charge region $\int_{-t_0}^{t_{dr}} dt = \int_0^w [1/\mu E(x, q_e, X_0)] dx$. The

temporal variation of the surface charge domain is clearly non-exponential, and should be described by the solution of a transcendental equation $q_e(t) = eN_{Def}w_q(t) - eN_{Def}X_0(t)/\{1 - \exp[-(t + t_0)/\tau_M]\}$. Here, t_0 is the duration of the induced carrier separation and formation of the q_e domain, $\tau_M = \epsilon_0\epsilon/(eN_{Def}\mu_e)$ is the dielectric relaxation time, e is the elementary charge, ϵ_0 and ϵ are vacuum and material permittivity, respectively, $N_{Def} = n_0$ is the effective doping density. Infinitely narrow injected surface-charge sketched by a dotted line in Fig. 4 is an idealisation.

In reality, a close to exponentially decreasing profile of the excess carrier density is induced by a light pulse. Thus, the excess carrier domain induced surface field can be found by combining the Poisson and Gauss integrals, and it can be evaluated as

$$E = en_{ex0}\alpha^{-1}[1 - \exp(-\alpha\Delta)]/(\epsilon_0\epsilon). \quad (2)$$

Here, α is the light absorption coefficient at the excitation wavelength, n_{ex0} is the excess carrier density photo-generated at the base layer surface, and Δ is the effective width of the light injected charge domain. The latter should be taken as $\Delta = 5\alpha^{-1}$ if the averaged carrier density is to be controlled with a precision of 1% relative to n_{ex0} . The solid line in Fig. 4 shows the electric field distribution including the spreading of the injected surface charge domain. This spreading of the injected surface charge domain is the main reason for the double peak formation, if the applied voltage approaches U_{FD} .

The first peak in the ICDC signal is again associated with excess hole extraction into the p^+ layer and simultaneous majority (p_0) hole extraction from the electrically neutral p^+ layer (with w_{p^+} increment) towards metallic electrode and external circuit. The second peak in the ICDC transient appears due to $w_q = d = w_{q,FD}$ at full depletion. At full depletion voltage (U_{FD}), the steady-state electric field is zero at $x_{FD} = w_{q,FD} - w_{0,FD}$. Thus, the last stage of excess carrier extraction runs within the increasing field region, i. e. self-acceleration of excess electrons appears to collapse the excess carrier domain at the external electrode (n^+ layer) (relatively to the base region). A similar (but opposite) effect appears in the extraction of excess holes from the n-base. These holes extracted and localized at the p^+ layer ($X_{0,p^+} < X_{0,n}$) reduce the steady-state field at $x = 0$ (by an extent $ep_{ex0}\alpha^{-1}/(\epsilon_0\epsilon)$) and slow down their

later extraction. Therefore, the ICDC initial peak is smoothed. The double peak transients inherent for ICDC are observed in Fig. 2(a). As discussed above, a rather “corrugated” electric field distribution appears for applied voltages $U \leq U_{\text{FD}}$. An enhancement of U above U_{FD} leads to an approximately uniform field distribution through the base of the pin diode, and the electric field is supported by planes of charge located at the external contact layers. The parallel plate condenser approximation can then be employed. At a fixed external voltage, electric field distribution within the considerably over-depleted base of the pin detector approaches a constant value independent of depth within the base region. Operation of the diode with injected charge becomes similar to that of a capacitor in this case.

The smoothing of the field at $U > U_{\text{FD}}$ enables one to simplify evaluation of the mobility of excess carriers by using the well-known relation $\mu_e = d^2/(\tau_{\text{tr}}U)$ and drift time τ_{tr} measurements within the ICDC pulse. To evaluate changes of material during irradiation, measurements of carrier mobility at excess carrier densities $n_{\text{ex}} < n_0$, close to that values measured in dark are preferable; therefore, the least possible excitation densities were maintained in our μ_e measurements. Commonly, the drift time is evaluated as the time interval for the time of flight (TOF) pulse (at $U > U_{\text{FD}}$, when $\tau_{\text{tr}} < \tau_{\text{M}}$). In our case, however, an initial delay appears within the risetime. This delay is caused by excess carrier temporal variations during laser pulse (τ_{L}) and by the measurement circuitry time constant $RC \approx 0.6$ ns. Actually, the rise time to peak τ_{r} should be taken as $\tau_{\text{r}} = 5RC$, to increase precision. The value of $\tau_{\text{r}} = 2.5\text{--}3$ ns is obtained in practice (Fig. 2(a)). Therefore, a more reliable way to extract τ_{tr} is from an estimation of the time interval between the ICDC peaks, which really indicates the steady state excess carrier generation and separation process. The extracted values of electron mobility $\mu_e = d^2/(\tau_{\text{tr}}U) \cong 1300$ cm²/(Vs) (for a non-irradiated sample) validate the chosen interval for the drift time measurement. The ICDC current amplitudes slightly decrease with irradiation exposure time (due to the capture of carriers on radiation induced traps), while drift time is nearly invariant, as shown in Fig. 2(b). The mobility value variations $\Delta\mu/\mu < 20\%$, estimated from the dispersion of τ_{tr} values during irradiation and illustrated in Fig. 2(b), show a small impact of irradiation on the carrier scattering parameters. This

is in qualitative agreement with results published in [6–8], while absolute values of μ_e obtained during irradiation appear to be lower than the value $\mu_e = 1600\text{--}2000$ cm²/(Vs) evaluated after irradiation [6, 8] and $\mu_e = 1000\text{--}1200$ cm²/(Vs) published in [7]. The explanation might be the different models exploited for the extraction of μ_e values and the injected excess carrier domain width Δ .

The ICD current associated with the injected excess electron charge domain for $U \leq U_{\text{FD}}$ varies due to temporal changes in $w_q(t)$. As $w_q(t)$ contains the product of the induced charge relaxation $q_e(t)$ (due to carrier capture to traps) and the pair separation length $X_0(t)$ parameters and the space charge density $N_{\text{Def}}(t)$ changes (due to fast thermal emission from filled traps), the ICD current is generally composed of three components. Using the depletion approximation, this is

$$i_{\text{ICD}}(t) = \frac{C(t)U}{2} \frac{\left(w_q(t) \Big|_{U=0} \right)^2}{w_q^2(t)} \left[(\mp) \frac{v_q(t)}{X_0(t)} + \frac{1}{\tau_{\text{capt}}} + \frac{w_q^2(t)}{\left(w_q(t) \Big|_{U=0} \right)^2} \frac{(\pm)n_d(t)}{N_{\text{Def}}(t)} \frac{1}{\tau_g} \right]. \quad (3)$$

Here, additional symbols represent: $C(t) = \epsilon_0 \epsilon S/w_q(t)$, τ_{capt} is the excess carrier (q_e) capture lifetime within depleted region, τ_g is the carrier thermal emission lifetime within depleted region, $n_d(t) = n_{\text{d0}} \exp(-t/\tau_g)$ is the density of carriers trapped on fast emission centres, $[w_q(t)|_{U=0}]^2 = 2q_e X_0/eN_{\text{Def}}$, S is the area of a junction. The first component in $i_{\text{ICD}}(t)$ represents variations of separation length (for $v_q = dX_0/dt \neq 0$), and it is analogous to Ramo’s [17] current within dielectric space between plates of the capacitor. To keep this analogy, a possibility of both (\mp) directions of drift current is denoted in Eq. (3), depending on the induced charge sign and on the direction of the charged particle motion. The expression of this displacement current component, due to the drift of the charge domain within the space charge region of a diode, is more complicated than that for the Ramo’s current ($i = ev/w$) [13, 17], and it is governed by the barrier capacitance $C(t)$ temporal changes and depends on the ratio of the depletion width changes caused by the moving charge domain q_e and normalised to space charge eN_{Def} as

$[2q_e X_0 / (eN_{\text{Deff}})] / [2\varepsilon\varepsilon_0 / (eN_{\text{Deff}}) (U + q_e X_0 / (\varepsilon\varepsilon_0))]$. The second component of current within Eq. (3) is ascribed to the excess carrier capture process (for $dq_e / dt = edn_{\text{ex},s} / dt = -en_{\text{ex},s} / \tau_{\text{capt}}$) within the depleted n -base region. It can be also deduced that an enhancement of excess carrier density (of the $2en_{\text{ex}} / eN_D$) would be preferential to clarify the excess electrons trapping processes. The third component in Eq. (3) appears when the influence of the fast carrier generation centres within the space charge region is significant. Here, both (\pm) donor (+) and acceptor (–) type traps can be involved. The impact of the slow (deep) generation centres appears as a leakage current $i_{\text{gl}}(t) = en_1 w_q(t) S / \tau_{\text{gl}}$. Including recombination/diffusion i_{R} [16] currents within n^+ and p^+ layers, the total diode current $i_{\Sigma}(t)$ can be expressed through the sum of the mentioned components: $i_{\Sigma}(t) = i_{\text{ICDC}}(t) + i_{\text{gl}}(t) + i_{\text{R}}(t)$.

There are several regimes of ICD current measurements (to clarify carrier capture/diffusion) depending on the ratio en_{ex} / eN_D . The n_{ex} density also determines the fraction of carriers (n_{tr}) which can be moved by the electrical field of the depleted barrier capacitance. For $n_{\text{ex}} \rightarrow n_0 = N_D$ and $U \leq U_{\text{FD}}$, the current contains components dq_e / dt and dX_0 / dt , due to the external electric field during initial instants and the ambipolar diffusion of the quasi-neutral domain of excess carriers after this electric field is screened. As a measure for the ratio of the carrier density which decays through carrier diffusion–recombination ($n_{\text{D-R}}$) and of that which disappears from the depletion region via drift (n_{tr}) can be a threshold value of charge affordable to shift by applied dc external voltage. Carrier density involved in charge transit is evaluated by using the depletion approximation for a parallel plate capacitor of area S , and expressed as

$$n_{\text{tr}} = \varepsilon\varepsilon_0 U / (ew_q \Delta). \quad (4)$$

Actually, the external electric field is rapidly screened (during a dielectric relaxation or transit time $\tau_{\text{tr}} = d^2 / \mu U$ for carriers of mobility μ , if $\tau_{\text{tr}} \ll \tau_{\text{R}}$) owing to light generated excess carriers $n_{\text{ex}0}$, and n_{tr} vanishes ($n_{\text{tr}} \rightarrow 0$) within the initial transient stages if $n_{\text{ex}0} \approx n_0$ is sufficiently large. The light induced domain of excess electrons is then able to dissipate through (be collected at) the n^+ electrode due to diffusion across the base and carrier extraction by the electric field at the external electrode. The simplified approximation of the carrier domain drift

and diffusion process can be described by a classical expression [18] for carrier density variations dependent on time and position as

$$n_{\text{R-D}}(x, t) = (n_{\text{ex}0} - n_{\text{tr}}(t)) \frac{\Delta}{\sqrt{4\pi D_A t}} \exp\left\{-\left[\frac{(x - \mu Et)^2}{4D_A t} + \frac{t}{\tau_{\text{R}}}\right]\right\}. \quad (5)$$

Here, $n_{\text{ex}0}$ is the initial ($t = 0$) density of bipolar photo-excited carriers, D_A is the coefficient of carrier ambipolar diffusion. Depending on the probing regime (either IChCC or MW-PC-E) the signal is sensitive either to carrier density at the collecting electrode $n_{\text{R-D}}(t, d)$ or depth integrated carrier density $(1/d) \int_0^d n_{\text{R-D}}(t, x) dx$ for IChCC or MW-PCT-E response, respectively. In the pin diode, n^+ electrode collects electrons (and blocks holes), hence the injected charge collection current (IChCC) is measured. The MW-PC transient appears as a relaxation pulse with a vertex characterised by the descending slope of a trapezium-like pulse serving for the extraction of recombination lifetime.

At a rather high excitation density, $en_{\text{ex}} \Delta > CU$, and low applied voltage, the IChC current transient acquires a rising peak pulse shape with a very small amplitude at initial instants and effective lifetime at the IChCC pulse vertex evaluated as $\tau_s = (\tau_{\text{D}}^{-1} + \tau_{\text{R}}^{-1})^{-1}$ with carrier recombination (τ_{R}) and diffusion $\tau_{\text{D}} \cong d^2 / (4\pi^2 D_A)$ times.

The values of $\tau_s = f(\tau_{\text{D}}, \tau_{\text{R}})$ estimated from the IChCC transients (Fig. 3(a)) and the parameters measured by the MW-PC-E technique (τ_{R} (Fig. 3(b)) and μ, τ_{D}) estimated from ICDC transients (Fig. 2(a)) are shown in Fig. 5 as a function of irradiation exposure time. Here, the leakage current proportional to the thermal emission/carrier detrapping within the space charge region current is presented. The reciprocal recombination lifetime (Fig. 5) increases with exposure time (irradiation fluence is assumed to be proportional to exposure time) nearly linearly during initial irradiation stages. At elevated fluences, however, values of the effective recombination lifetime τ_{R} measured by the MW-PC-E technique on diodes with applied electric field start to saturate. This can be easily understood by the manifestation of multi-trapping effects, when several (recombination and trapping) centres act together, due to effective point defect

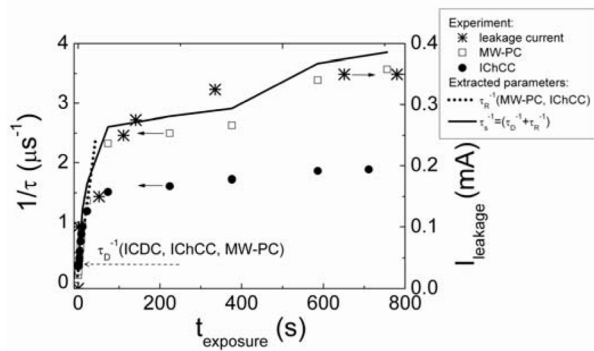


Fig. 5. Correlation among the carrier drift/diffusion, recombination and generation characteristics measured *in situ* (symbols) and calculated ones (lines). These characteristics were measured during 8 MeV proton irradiation of a Si detector by using the induced charge diode current (ICDC) and injected charge collection current (IChCC) transient method (circles) and by the technique of microwave probed photoconductivity with applied electric field (MW-PCT-E) (squares), respectively. Leakage current variations with fluence (stars) are also presented.

generation during irradiation by protons. The saturation of the effective recombination lifetime (which averages the carrier recombination and multi-trapping rate) correlates well with the enhancement of leakage current relative to the irradiation exposure time scale.

The presented techniques enable the estimation of variations of the excess carrier drift and trapping parameters. However, improved precision in extracting parameters on high-resistivity material is limited by the long Debye length for Si ($5L_D \geq 40 \mu\text{m}$ for 1 k Ωcm Si) in the evaluation of the steady-state depletion width, and by the finite width of the injected excess carrier domain ($\Delta > 6 \mu\text{m}$ for excitation wavelength 531 nm and $\Delta > 80 \mu\text{m}$ for red light). These widths also limit the precision in evaluating the depletion voltage values.

5. Conclusions

A multi-functional instrument and techniques suitable for simultaneous monitoring of the evolution of radiation defects and of changing functional characteristics of Si particle detectors during irradiation with protons have been tested. A

small impact of radiation defects has been revealed on drift/diffusion parameters of carriers of both signs and more complex variations of excess carrier recombination and trapping lifetimes during irradiation. Models have been proposed for an under-depleted diode with induced charge and of current transients at low and high densities of light excited excess carriers within the diode base region. The excess carrier transit, recombination and diffusion lifetimes have been evaluated by combining ICDC/IChCC current and microwave-probed photoconductivity transient techniques. It has been shown that the values of the effective recombination lifetime measured by the MW-PC-E technique on diodes with applied electric field start to saturate. This saturation is explained as the manifestation of multi-trapping effects, when several centres of different species act together. The saturation of the effective recombination lifetime, which averages the carrier recombination and multi-trapping rate, correlates well with the enhancement of leakage current relative to the irradiation exposure time scale.

Acknowledgements

The authors appreciate J. Harkonen and E. Tuominen for provided Si pad-detectors. J. Kaladé and G. Juška are acknowledged for fruitful discussions on the theoretical and phenomenological aspects of carrier transport. A. Uleckas is acknowledged for the design of software for ICDC-IChCC measurement instrument and help in experiments. This work has been performed in the frame of the CERN-RD39 collaboration. The financial support of the Academy of Finland (Project No. 132128) is gratefully acknowledged.

References

- [1] I. Pintilie, E. Fretwurst, G. Lindström, and J. Stahl, Second-order generation of point defects in gamma-irradiated float-zone silicon, an explanation for “type inversion”, *Appl. Phys. Lett.* **82**, 2169–2171 (2003).
- [2] M. Mikelsen, J.H. Bleka, J.S. Christensen, E.V. Monakhov, B.G. Svensson, J. Harkonen, and B. Avset, Annealing of the divacancy-oxygen and vacancy-oxygen complexes in silicon, *Phys. Rev. B* **75**, 155202 (2007).

- [3] M. Scaringella, D. Menichelli, A. Candelori, R. Rando, and M. Bruzzi, Defect characterization in silicon particle detectors irradiated with Li ions, *IEEE Trans. Nucl. Sci.* **53**, 589–594 (2006).
- [4] V. Eremin, N. Strokan, E. Verbitskaya, and Z. Li, Development of transient current and charge techniques for the measurement of effective net concentration of ionized charges (N_{eff}) in the space charge region of p-n junction detectors, *Nucl. Instrum. Methods A* **372**, 388–398 (1996).
- [5] J. Härkönen, V. Eremin, E. Verbitskaya, S. Czellar, P. Pusa, Z. Li, and T.O. Niinikoski, The cryogenic transient current technique (C-TCT) measurement setup of CERN RD39 collaboration, *Nucl. Instrum. Methods A* **581**, 347–350 (2007).
- [6] V. Eremin and Z. Li, Carrier drift mobility study in neutron irradiated high purity silicon, *Nucl. Instrum. Methods A* **362**, 338–343 (1995).
- [7] C. Leroy, P. Roy, G. Casse, M. Glaser, E. Grigoriev, and F. Lemeilleur, Study of charge transport in non-irradiated and irradiated silicon detectors, *Nucl. Instrum. Methods A* **426**, 99–108 (1999).
- [8] T.J. Brodbeck, A. Chilingarov, T. Sloan, E. Fretwurst, M. Kuhnke, and G. Lindstroem, Carrier mobilities in irradiated silicon, *Nucl. Instrum. Methods A* **477**, 287–282 (2002).
- [9] E. Gaubas, A. Uleckas, J. Vaitkus, J. Raisanen, and P. Tikkanen, Instrumentation for the *in situ* control of carrier recombination characteristics during irradiation by protons, *Rev. Sci. Instrum.* **81**, 053303 (2010).
- [10] S. Väyrynen, J. Räisänen, I. Kassamakov, and E. Tuominen, Breakdown of silicon particle detectors under proton irradiation, *J. Appl. Phys.* **106**, 104914 (2009).
- [11] G. Cavalleri, E. Gatti, G. Fabri, and V. Svelto, Extension of Ramo's theorem as applied to induced charge in semiconductor detectors, *Nucl. Instrum. Methods* **92**, 137–140 (1971).
- [12] P. De Visschere, The validity of Ramo's theorem, *Solid State Electron.* **33**, 455–459 (1990).
- [13] L.-A. Hamel and M. Julien, Generalized demonstration of Ramo's theorem with space charge and polarization effects, *Nucl. Instrum. Methods A* **597**, 207–211 (2008).
- [14] I.V. Kotov, Currents induced by charges moving in semiconductor, *Nucl. Instrum. Methods A* **539**, 267–268 (2005).
- [15] P. Blood and J.W. Orton, *The Electrical Characterization of Semiconductors: Majority Carriers and Electron States* (Academic Press, London – San Diego – New York, 1992).
- [16] B.Y. Baliga, *Power Semiconductor Devices* (PWS Publishing Company, Boston, 1995).
- [17] S. Ramo, Currents induced by electron motion, *Proc. Inst. Radio Eng.* **27**, 584–585 (1939).
- [18] R. Smith, *Semiconductors*, 2nd ed. (Cambridge Univ. Press, London – New York, 1982).

KRŪVININKŲ DREIFO IR DIFUZIJOS ŠI DALELIŲ DETEKTORIUOSE CHARAKTERISTIKOS, IŠMATUOTOS 8 MeV PROTONŲ APŠVITOS METU

E. Gaubas ^a, T. Čeponis ^a, J. Vaitkus ^a, J. Raisanen ^b

^aVilniaus universiteto Taikomųjų mokslų institutas, Vilnius, Lietuva

^bHelsinkio universiteto Fizikos skyriaus Medžiagų fizikos sektorius, Helsinkis, Suomija

Santrauka

Krūvininkų dreifo ir difuzijos charakteristikos lemia aukštųjų energijų dalelių detektorių funkcinis parametras. Šiame darbe aptarta *in situ* kontrolės įranga difuzijos-dreifo parametrams, švitinant 8 MeV energijos protonais, įvertinti. Ši įranga pagrįsta mikrobangomis zonduojamo fotolaidumo ir krūvio surinkimo kinetinių vienalaikiams matavimais pridėjus užtvarinę įtampą. Įvertinta, kad elektronų judris beveik nepriklauso nuo apšvitos protonais įtėkio, o elektronų judrio vertė yra $\mu_e \cong 1300 \text{ cm}^2/\text{Vs}$. Krūvininkų rekombinacijos trukmė

mažėja tiesiškai pradinių apšvitos protonais ekspozicijų intervale, tačiau pradeda sotintis tęsiant apšvitą didelių įtėkių srityje. Tai paaiškinta daugkartinio krūvininkų prilipimo procesais, kai veikia keletas centrų (prilipimo ir rekombinacinių) apšvitos metu formuojantis taškiniais defektams. Eksperimentinių rezultatų analizei pasiūlyti srovės kinetinių modelių, kai yra pridėtos įtampos iki ir virš visiško detektoriaus bazės nusukordinimo. Taip pat sumodeliuotos krūvio surinkimo srovės kinetikos esant įvairiems nepusiausvirųjų krūvininkų tankiams.